

# We are IntechOpen, the world's leading publisher of Open Access books Built by scientists, for scientists

4,400

Open access books available

117,000

International authors and editors

130M

Downloads

Our authors are among the

154

Countries delivered to

TOP 1%

most cited scientists

12.2%

Contributors from top 500 universities



WEB OF SCIENCE™

Selection of our books indexed in the Book Citation Index  
in Web of Science™ Core Collection (BKCI)

Interested in publishing with us?  
Contact [book.department@intechopen.com](mailto:book.department@intechopen.com)

Numbers displayed above are based on latest data collected.  
For more information visit [www.intechopen.com](http://www.intechopen.com)



---

# X-Ray Photoelectron Spectroscopy for Characterization of Engineered Elastomer Surfaces

---

Lidia Martínez, Elisa Román and Roman Nevshupa

Additional information is available at the end of the chapter

<http://dx.doi.org/10.5772/48101>

---

## 1. Introduction

Among different types of polymers, elastomers, also called rubbers, are of special interest for many industrial applications. This interest resides in the high yield strength of these materials that makes possible deforming them manifold their original length without permanent residual strain. However, elastomers can suffer from surface deterioration when subject to rubbing, contacting with aggressive media, ultraviolet light and other. Oxidation of elastomers can produce degradation of its chemical, physico-mechanical, rheological and surface properties. In tribological applications, the quality of the elastomer surfaces is also of special concern since significant degradation of mechanical and tribological behaviour is usually associated with small changes in the surface composition and properties [1]. Therefore, studying the mechanisms of surface degradation of elastomers is very important for comprehension of the failure modes of elastomer components and improving their durability.

For improving the performance of material surfaces, different surface modifications have been developed so far. Properties of elastomer surfaces depend, to a large degree, on the chemical constitution of molecules in the surface layer [2]. Therefore, tailoring polymer surfaces has attracted much interest of researchers in polymer chemistry [3]. Polymer surface modification allows obtaining good performance of components at lower costs than using expensive advanced bulk materials [4]. Presently, halogenation, etching, grafting, oxidation, and other surface modification techniques are intensively used. Another alternative is the application of coatings onto the elastomer surface, although the application of coatings on deformable substrates without occurrence of interfacial delamination is not straightforward. Among various coatings, amorphous diamond-like carbon (DLC) is considered by various authors as a good candidate for application on elastomer surfaces [5]. Such coatings have excellent tribological behaviour, i.e., low friction coefficient and wear rate [6].

Ethylene-propylene-diene elastomer (EPDM) is one of the most widely used elastomers in various outdoor and industrial applications, such as waterproof coatings, electrical insulation, pipes, and mounts. In general, it is employed in applications which demand a material with good mechanical properties and with a retained elastic nature [7]. World production of EPDM is estimated to be 41% of all elastomers [8-11]. Also it has a good resistance to degradation at elevated temperature, sunlight, in oxygen and, in particular, ozone [12]. Acrylonitrile-butadiene rubbers (NBR) and hydrogenated acrylonitrile-butadiene rubbers (HNBR) form another widely used family of elastomers. In hydrogenated rubber the double bonds of butadiene ( $\text{CH}_2=\text{CH}-\text{C}\equiv\text{N}$ ) are saturated yielding rubber with much higher chemical inertness. These elastomers are extensively employed in automotive industry, especially for lip seals, due to their moderate cost, excellent resistance to oils, fuels and greases, processability and very good resistance to swelling by aliphatic hydrocarbons [13].

Our study is focused on characterization of surface chemical composition of different elastomers subject to rubbing, surface modification and application of coatings. The main technique used for this study was X-ray photoelectron spectroscopy (XPS), which is a very powerful technique for characterizing the chemical composition of very thin (few nm) surface layers. XPS is particularly useful when analysing elastomers, as it provides information about the chemical environment of the elements, i.e. type of bonds, chemical state, etc. Thus, XPS is well suited for investigation the changes in binding energy of chemical elements situated within the first tens of nanometres of the material surface [4]. Elastomers are typically composed of carbon, hydrogen, oxygen and nitrogen. Their surface and bulk properties depend on the way these elements are combined rather than on the presence of other chemical elements. XPS allows detection of new functional groups [4] and evaluation the variation in the amount of existing functional groups, e.g. C-O, as function of surface tailoring, ageing [1], or rubbing [14]. However, often it can be difficult to distinguish between different functional groups having similar binding energies. Therefore, in many cases some complementary techniques should be used to elucidate chemical features of elastomer surfaces. One of these complementary techniques consists in measuring of contact angles (CA) of sessile drops of various liquids placed on the elastomer surface. This very simple method provides valuable information on the types of surface groups [15]. In particular, by using water, presence of polar groups, e.g. C-O, can be determined. So, the degree of surface activation due to surface modification can be determined from measurements of surface hydrophobicity [16]. Then, more information on the surface chemistry and Surface Free Energy (SFE) can be obtained from measuring CA of various liquids with different characteristics. In the following sections we present some fundamental aspects of these techniques and case studies of elastomer surfaces.

## 2. XPS for characterization of elastomer surfaces

### 2.1. Introduction to the XPS technique

XPS is an analytical technique that has its fundamental origin in the photoelectric effect, which was first explained by Einstein in 1905 [17]. This effect has become a powerful tool for

studying the composition and the electronic structure of the matter [18]. A schematic drawing of typical XPS measurement device is shown in Figure 1a. The measurements are performed in ultrahigh vacuum (UHV) in order to control the surface cleanliness and to reduce the electron scattering on gas molecules. To provide a beam of photons with given characteristics the device is equipped with an X-ray source focused on the sample surface. The photoelectrons emitted from the sample material at characteristic energies are analysed by a suitable electron analyser. The kinetic energy,  $E_k$ , at which electrons are emitted follows the fundamental energy conservation equation in photoemission:

$$h\nu = E_B + E_K + \phi_a, \quad (1)$$

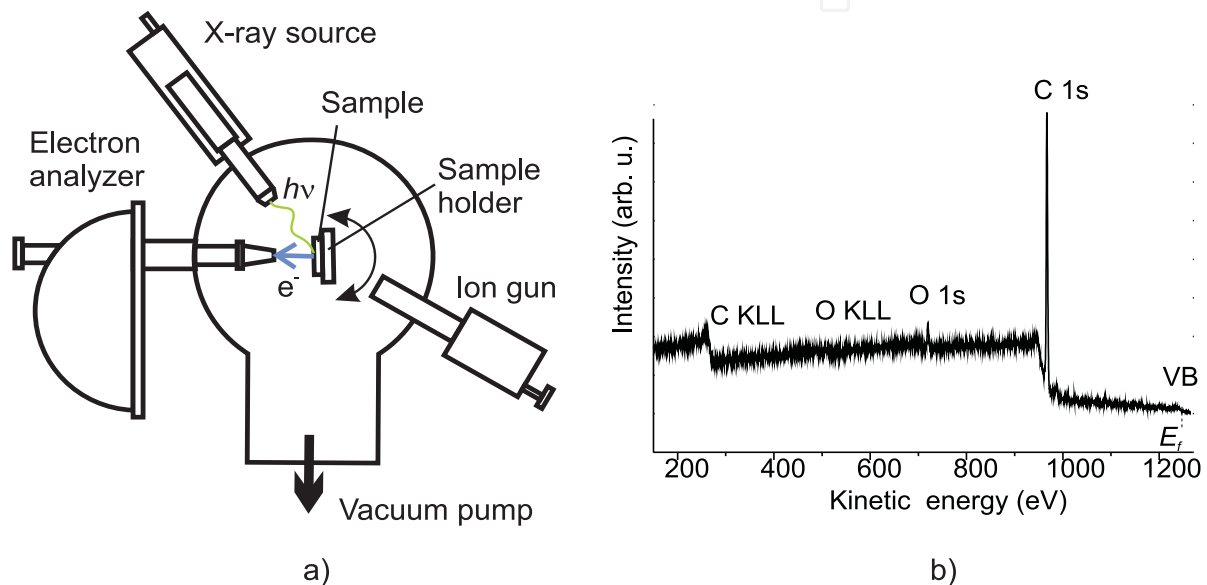


**Figure 1.** a) Schematic drawing of an experimental XPS system; b) typical photoemission spectra of an elastomer

in which  $h$  is Plank constant;  $\nu$  is the photon frequency and the product  $h\nu$  defines the energy of the incident photon;  $E_B$  is the binding energy of the electron in the atom. The origin of the binding energies is related with Fermi level,  $E_f$ , whereas the kinetic energies are referenced to the vacuum level. The difference between both levels corresponds to work function of the analyser,  $\phi_a$ . By measuring the electron kinetic energies and knowing the spectrometer work function, it is possible to determine the binding energies of various inner levels (or core electrons), as well as those of the outer (or valence) electrons involved in chemical bonding. A typical photoemission (PE) spectrum, i.e. PE yield vs. kinetic energy of the emitted photoelectrons obtained from a photon-illuminated area, is shown in Figure 1b. The spectrum consists of a series of peaks on a background signal which generally increases at low kinetic energy due to secondary electrons, i.e. photoelectrons that are inelastically scattered in the way out of the sample. In summary, the XPS spectra consist of peaks at discrete kinetic energies corresponding to atomic core levels (CLs) and Auger transitions. Note that each element has a unique elemental spectrum. With the most commonly used excitation sources, the kinetic energy of photoelectrons is typically ranged between 0 and

1400 eV. Since inelastic mean free path of photoelectrons,  $\lambda$ , in solids is small [19], chemical information is obtained from the surface and few subsurface atomic layers. Quantitative information can be derived from the peaks areas, whereas chemical states can often be identified from the exact positions of the peaks and separations between them. The presence of chemical bonding causes binding energy shifts, which can be used to infer the chemical nature (such as atomic oxidation state) from the sample surface. Here, we limit ourselves to study elastomer samples. A complete description of XPS technique can be found in specialized literature [20, 21].

## 2.2. Advantages and shortcomings of XPS technique for characterization of elastomer surfaces. Operating conditions, measurements and semi-quantitative analysis

The standard XPS measurements are carried out under vacuum conditions by retarding-fields techniques. The most commonly used X-ray sources are Al K $\alpha$  (1486.6 eV) and Mg K $\alpha$  (1253.6 eV). The X-ray lines from these sources are narrow (less than 0.9 eV) and provide good energy resolution for many applications. Initially, a survey scan or wide energy range scan, typically from 1000 to 0 eV, should be obtained in order to identify the elements present on the surface. As each element emits electrons at characteristic energies, it is possible to identify all the elements present in the sample surface, except hydrogen and helium which are not detectable by this technique. Elastomers usually contain a small number of elements, of which the most common are C, O, N, F and Cl. Other elements like sulphur and zinc can be detected in small quantities. Sulphur is a typical curing agent, whereas zinc is usually employed as a curing activator [22]. In most of the cases, these elements will not be taken into account as they have no real influence on the surfaces properties. Normally, the elements are uniformly distributed in the bulk; however, under certain circumstances surface segregation may take place.

It should be stressed that XPS is a semi-quantitative technique. In order to quantify the amount of each element the integrated area of a particular peak should be divided by the corresponding relative sensitivity factor. The following is a generalized expression for determination of atom fraction,  $C_x$ , of a constituent  $x$  in a sample:

$$C_x = (I_x / S_x) / (\sum I_i / S_i), \quad (2)$$

where  $I_x$  is the peak area and  $S_x$  is the atomic sensitivity factor of the  $x$ -th element. The denominator corresponds to the atomic fraction of other elements in the sample. Assuming a homogeneous distribution of elements, a strong line for each element in the spectrum should be analyzed. In case the requirement of homogeneity is not fulfilled, the assumption of homogeneity can be used as a starting point for further calculations. Reference published data on elemental sensitivity factors could be used for determination of  $S$ , although the type of instrument and analysis conditions should be considered. With this technique it is also possible to identify chemical states of a given element by measuring the high resolution or core level peaks.

Depth distribution of elements can also be obtained using XPS in destructive or non-destructive modes. In the first one, ion sputtering is used to remove surface layers. Sputtering and XPS can be applied consecutively or simultaneously. In the non-destructive mode, depth profiling is obtained by varying the detection angle of the emitted electrons. In this case the probed depth is limited to  $3\lambda$ . More detailed information about both methods can be found elsewhere [20].

Another important problem in XPS analysis is related with sample degradation due to X-ray radiation. In fact, this degradation comes from the secondary electrons emitted during the X-ray exposure [23, 24]. In most of the cases this degradation is slow enough as compared with time required for XPS analysis, thus the changes in composition due to X-ray can be neglected. Notwithstanding, this problem should be considered when analysing chemically unstable materials. In our work, no sample degradation due to X-ray radiation has been observed for all studied elastomers.

XPS measurements were performed in ultrahigh vacuum with base pressure of  $2 \times 10^{-10}$  mbar using a Phoibos 100 ESCA/Auger spectrometer with Mg  $K\alpha$  anode (1253.6 eV). To avoid X-ray damage on the samples low X-ray power of 150 W was used. The core level narrow spectra were recorded using pass energy of 15 eV. For the data analysis, the contributions of the Mg  $K\alpha$  satellite lines were subtracted and the spectra were subjected to a Shirley background subtraction formalism [25]. The binding energy,  $E_B$ , scale was calibrated with respect to the C 1s core level peak at 285 eV. The surface area subject to XPS analysis was around 5.6 mm<sup>2</sup> that is large enough to obtain an average surface chemical composition. When modified samples were analyzed, the surface area subject to XPS analysis was smaller than the treated area, thus the contribution from untreated surfaces was negligible. The shape of C 1s core level peak (HR C1s) measured with high energy resolution was analysed using peak fitting in order to identify functional groups. Depending on the chemical environment of the carbon atoms, important chemical shift of C 1s peak can be observed. Decomposition of the experimental peak in components allows identification of the contribution from each component. For the analysis of HR C1s, the spectrum recorded from the untreated sample was used as a reference. The HR C1s was fitted leaving the full width at half maximum (FWHM) of the C–C/C–H component to vary freely while the other components were forced to adopt the same value. The fit of the treated samples was performed using the same values of FWHM and the binding energies (with uncertainty of  $\pm 0.1$  eV) as for untreated elastomer. The only remaining free parameter in the fit procedure was the area of the peaks. By doing so, new carbon species derived from the treatment processes could be identified. An example of the analysis of HR C1s is presented in Figure 2 where some spectra of untreated and modified elastomers are compared. Presence of new carbon species (in this case C–O and C–F bonds) can be identified from the shape of the HR C1s. The contribution from these groups varied depending on the surface treatment. However, identification of chemical groups can be difficult when different species produce similar chemical shifts (see Table 1 for  $E_B$  of main carbon bonds identified in the present study). For example, C=C bond was included into the group of C–C/ C–H components since the shift between these two groups is only 0.3 eV [26] that is below the resolution limit of the

experimental system used in this study. Detailed analysis of XPS spectra is presented in section 3.3.

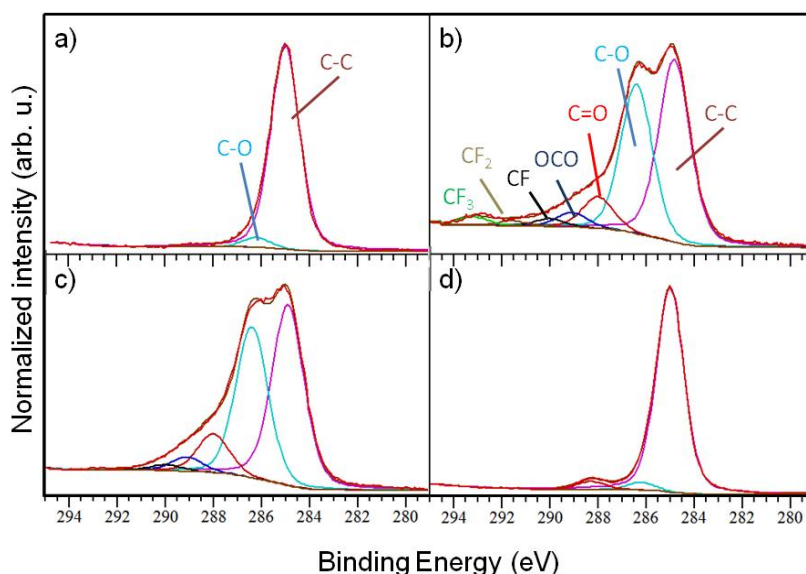


**Figure 2.** High resolution C1s core level spectra of elastomer samples: a) untreated EPDM, b) EPDM after fluorination with  $\text{CF}_4$ , c) EPDM after fluorination with  $\text{SF}_6$ , and d) HNBR after the same fluorination as c)

Bonds	$E_B$ ( $\pm 0.1$ eV)	Ref.
C-C, C-H, C=C	285	[26, 27]
C-O, -CH- $\text{CF}_2$	286.3	[26-30]
C=O, -CH-CF	288.1	[26-30]
O-C=O, -CFH- $\text{CF}_2$	289	[26-30]
CF	289.8	[30, 31]
$\text{CF}_2$	291.8	[30, 31]
$\text{CF}_3$	293.3	[30-32]

**Table 1.** Components employed for the analysis of the C 1s core levels

### 2.3. Complementary techniques for the interpretation of the results of XPS

As we mentioned in the introduction section, surface and bulk properties of elastomers depend on the way the main constituents (C, H, O, N, etc.) are combined rather than on the presence of other chemical elements. Therefore, in some cases and depending on the light source employed for XPS analysis, it is difficult to distinguish between the presence of different functional groups, as occurs for HR C1s with C-O and C-N groups. Complementary information on surface chemistry of elastomers can be obtained from spectroscopy of inelastic scattering of light, e.g. Fourier Transformed Infra-Red spectroscopy (FTIR), Raman spectroscopy and others. Measurements of SFE of elastomer using sessile drop method is another very simple but powerful method which can provide valuable information on the type of the surface groups. The method is based on

measuring the CA between a droplet of a certain liquid and an elastomer surface under well-controlled conditions. The CA is obtained from a balance of interfacial tensions between three phases: solid (S), liquid (L) and vapour (V) (Figure 3) and is defined from Young-Dupré equation:

$$\gamma_{SV} - \gamma_{SL} - \gamma_{LV} \cos \theta = 0 . \quad (3)$$

When a droplet contacts a rough surface, the measured or apparent contact angle, may differ from the intrinsic one, i.e. the CA of the same liquid on an ideally smooth surface of the same material. Wenzel [33] proposed to introduce a roughness factor,  $r$ , which is the real contact area divided by the geometrical, or projected, area. Homogeneous wetting regime of a liquid on a rough surface is described by:

$$r \cos \theta_a = \cos \theta . \quad (4)$$

The roughness factor can be determined numerically from 3D surface measurements obtained using appropriate technique, e.g. confocal microscopy, laser scanning profilometry, etc. [1]. Recently there were many criticisms on the Wenzel's approach. In [34] it was demonstrated that CA behaviour is determined by interactions of the liquid and the solid at the three-phase contact line alone and that the interfacial area within the perimeter is irrelevant. They suggested that Wenzel's equation is valid only to the extent that the structure of the contact area reflects the ground-state energies of contact lines and the transition states between them.

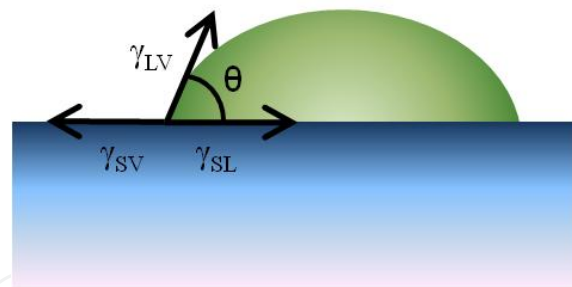


**Figure 3.** Schematic representation of contact angle

Depending on the specific method, the CA measurement allows determining total SFE, the polar and dispersive components of SFE (Fowke's approach), apolar Lifshitz – Van der Waals (LW) and polar acid - base components (van Oss's approach). According to van Oss's approach, the surface tension could be resolved into components due to dispersion, induction and dipole-dipole forces, and hydrogen bonding [35]. For non-metallic solid surfaces, in addition to apolar LW interactions, electron acceptor – electron donor interactions, or Lewis acid-base (AB) interactions may often occur. In this case the total surface tension is the sum of two components:  $\gamma^{LW}$  and  $\gamma^{AB}$  [36]. Unlike LW interactions, polar interactions are essentially asymmetrical. The polar component of the free energy of interaction between solid and liquid can be expressed as [35]:

$$\Delta F_{SL}^{AB} = -2 \left( \sqrt{\gamma_S^+ \gamma_L^-} + \sqrt{\gamma_S^- \gamma_L^+} \right), \quad (5)$$

where  $\gamma^+$  is the electron acceptor, or Lewis acid component, and  $\gamma$  is the electron donor, or Lewis base component of the surface tension. Then, the expanded form of Young-Dupré equation can be obtained by combining (3) and (5):

$$0.5\gamma_L^t (1 + \cos\theta) = \sqrt{\gamma_S^{LW} \gamma_L^{LW}} + \sqrt{\gamma_S^- \gamma_L^+} + \sqrt{\gamma_S^+ \gamma_L^-}. \quad (6)$$

If for a given liquid the components of surface tension  $\gamma_L^t$ ,  $\gamma_L^{LW}$ ,  $\gamma_L^+$ , and  $\gamma_L^-$  are known, (6) is a linear function of three unknown parameters corresponding to the components of surface tension of the solid surface  $\sqrt{\gamma_S^{LW}}$ ,  $\sqrt{\gamma_S^-}$ , and  $\sqrt{\gamma_S^+}$ . As this equation is underdetermined, the components of surface tension for the solid can be found by measuring CAs using at least three different liquids with known and different components of surface tension. If the values of the components of surface tension for the three liquids are close together, the calculated values for three parameters for the solid will be “unduly sensitive” [36] to small errors in the values of the parameters of surface tension of the liquids, and in the measured CAs. To overcome this problem, CA measurements should be performed with more than three liquids. These will constitute an overdetermined system of linear equations which can be solved by least-square method. In order to reduce the measurement error, each measurement of the CA should be repeated several times. Mean value,  $\bar{\theta}_i$ , and standard error of mean,  $se\theta_i$ , should be determined for each liquid from these measurements.

The resulting set of simultaneous equations is the following:

$$0.5\gamma_{Li}^t (1 + \cos\bar{\theta}_i) = \sqrt{\gamma_S^{LW} \gamma_{Li}^{LW}} + \sqrt{\gamma_S^- \gamma_{Li}^+} + \sqrt{\gamma_S^+ \gamma_{Li}^-}, \quad (7)$$

where subscript  $i$  indicates the liquid. It can be written in the matrix form:

$$\mathbf{Y} = \mathbf{A}\mathbf{b}, \quad (8)$$

where  $\mathbf{Y}$  is the matrix of independent variable (left side of eq. (7)),  $\mathbf{A}$  is the  $(n \times 3)$  matrix of known coefficients,  $n$  is the number of liquids used for CA measurements, and  $\mathbf{b}$  is the vector of unknown parameters:

$$\mathbf{Y} = 0.5 \left[ \left( 1 + \cos\bar{\theta}_1 \right) \gamma_{L1}^t \cdots \left( 1 + \cos\bar{\theta}_n \right) \gamma_{Ln}^t \right]^T, \quad (9)$$

$$\mathbf{A} = \begin{pmatrix} \sqrt{\gamma_{L1}^{LW}} & \sqrt{\gamma_{L1}^+} & \sqrt{\gamma_{L1}^-} \\ \cdot & \cdot & \cdot \\ \sqrt{\gamma_{Ln}^{LW}} & \sqrt{\gamma_{Ln}^+} & \sqrt{\gamma_{Ln}^-} \end{pmatrix}, \quad (10)$$

$$\mathbf{b} = \left[ \sqrt{\gamma_S^{LW}} \sqrt{\gamma_S^-} \sqrt{\gamma_S^+} \right]^T. \quad (11)$$

Then, mean values of the surface tension components can be determined from the matrix equation:

$$\mathbf{b} = (\mathbf{A}^T \mathbf{D}^{-1} \mathbf{A})^{-1} \mathbf{A}^T \mathbf{D}^{-1} \mathbf{Y}, \quad (12)$$

where  $\mathbf{D} = \begin{pmatrix} (se\theta_1)^2 & 0 & \mathbf{0} \\ 0 & \ddots & 0 \\ \mathbf{0} & 0 & (se\theta_n)^2 \end{pmatrix}$

is the covariance matrix of errors of CA measurements.

The standard error of mean of the unknown parameters can be found from the main diagonal of the covariance matrix:

$$\mathbf{K} = (\mathbf{A}^T \mathbf{D}^{-1} \mathbf{A})^{-1}. \quad (13)$$

The calculated values of the parameters of the surface tension should be tested for statistical significance using *t*-test. In case some of the parameters are not statistically significant, it can be zero set and removed from  $\mathbf{b}$ . Then, the calculation should be repeated using modified matrix  $\mathbf{A}$ . By doing so, the standard error of the parameters of solid can be reduced.

Matrix method is also very useful for the analysis of surface tension variation in time, e.g. due to ageing. In this case, CA measurements are performed at different periods of time using a set of several liquids as described above. This constitutes a set of simultaneous equations at the selected points of time.

$$0.5\gamma_{Li}^t (1 + \cos\bar{\theta}_i(t_j)) = \sqrt{\gamma_S^{LW}(t_j)\gamma_{Li}^{LW}} + \sqrt{\gamma_S^-(t_j)\gamma_{Li}^+} + \sqrt{\gamma_S^+(t_j)\gamma_{Li}^-}. \quad (14)$$

Therefore,  $\mathbf{Y}$  and  $\mathbf{b}$  change to  $(n \times p)$  matrixes, where  $p$  is the number of time points:

$$\mathbf{Y} = 0.5 \begin{pmatrix} (1 + \cos\theta_{11})\gamma_{L1}^t & \cdots & (1 + \cos\theta_{1j})\gamma_{L1}^t & \cdots & (1 + \cos\theta_{1p})\gamma_{L1}^t \\ \vdots & \vdots & \vdots & \vdots & \vdots \\ (1 + \cos\theta_{n1})\gamma_{Ln}^t & \cdots & (1 + \cos\theta_{nj})\gamma_{Ln}^t & \cdots & (1 + \cos\theta_{np})\gamma_{Ln}^t \end{pmatrix}, \quad (15)$$

$$\mathbf{b} = \begin{pmatrix} \sqrt{\gamma_{S1}^{LW}} & \cdots & \sqrt{\gamma_{Sj}^{LW}} & \cdots & \sqrt{\gamma_{Sp}^{LW}} \\ \sqrt{\gamma_{S1}^-} & \cdots & \sqrt{\gamma_{Sj}^-} & \cdots & \sqrt{\gamma_{Sp}^-} \\ \sqrt{\gamma_{S1}^+} & \cdots & \sqrt{\gamma_{Sj}^+} & \cdots & \sqrt{\gamma_{Sp}^+} \end{pmatrix}. \quad (16)$$

Assuming that all measurements have the same error, the matrix of parameters of solid surface can be found from the following equation:

$$\mathbf{b} = (\mathbf{A}^T \mathbf{A})^{-1} \mathbf{A}^T \mathbf{Y}, \quad (17)$$

and standard errors of the unknown parameters can be found from the main diagonal of the covariance matrix:

$$\mathbf{K} = s^2 (\mathbf{A}^T \mathbf{A})^{-1}, \quad (18)$$

where  $s^2$  is the sample variance determined as:

$$s^2 = \frac{1}{n-p-1} (\mathbf{Y} - \mathbf{A}\mathbf{b})^T (\mathbf{Y} - \mathbf{A}\mathbf{b}). \quad (19)$$

Although different substances can be used as probe liquids, the following five liquids are the most widely used: water, glycerol, diiodomethane, formamide, and ethylene glycol [1, 29, 37, 38]. The values of the components of surface tension for these liquids are listed in Table 2.

Liquid	$\gamma^t$	$\gamma^{LW}$	$\gamma^{AB}$	$\gamma^-$	$\gamma^+$
Water	72.80	21.80	51.00	25.50	25.50
Glycerol	64.00	34.00	30.00	57.40	3.92
Formamide	58.00	39.00	19.00	39.60	2.28
Ethylene glycol	48.00	29.00	19.00	30.10	3.00
Diiodomethane	50.80	50.80	0.00	0.00	0.00

**Table 2.** The components of surface tension for different probe liquids (from [29, 37])

Additionally, the Fowke's model can be used to determine the polar and dispersive components of surface energy. The following is the set of simultaneous Young-Dupré equations corresponding to the measurements of the CA for  $p$  liquids at time  $t_j$ :

$$0.5\gamma_{Li}^t (1 + \cos \bar{\theta}_i(t_j)) = \sqrt{\gamma_S^d(t_j)\gamma_{Li}^d} + \sqrt{\gamma_S^p(t_j)\gamma_{Li}^p}, i = 1 \dots p. \quad (20)$$

Since there are two unknown parameters in this model, the number of liquids used for the CA measurements can be smaller than for van Oss's model. After corresponding modification of  $\mathbf{A}$  and  $\mathbf{b}$ , solution of (20) can be found by the matrix method described above.

### 3. Case studies

#### 3.1. Characterization of elastomer surface subject to ageing

Though synthetic elastomers like EPDM are very attractive to industry due to their high chemical stability and low permeability for water, they are sensitive to oxidation at elevated

temperatures. Understanding of the chemical mechanisms of elastomer degradation is a key for designing advanced elastomers with higher resistance to oxidative degradation. Therefore, XPS and SFE analysis were employed to elucidate chemical changes produced on EPDM elastomer surfaces due to ageing.

XPS wide energy range scans were obtained for EPDM samples aged at 80 °C and 120 °C during up to 100 days. Surface chemical composition of the samples determined from these spectra as a function of ageing duration is shown in Table 3. The high carbon content in all samples arises from the contribution from the backbone structure of the elastomer. Oxygen, nitrogen, silicon and zinc are generally attributed to curing agents, amine-based accelerators and additives [1, 14].

With the increasing ageing duration, the O/C ratio also increases (last column of Table 3). In addition, for both temperatures there was certain increase in nitrogen and silicon concentrations for the 100 days ageing. As XPS is a superficial analysis technique, the variation of these elements present in small amounts on the surface could be related to diffusion processes during ageing and segregation of impurities on the surface. Being a thermally activated process, migration of additives is faster at higher temperatures, thus surface concentration of silicon after ageing at 120 °C is higher than at 80 °C.

Thermal ageing		Composition (% at.)					O/C ratio
$T$ (°C)	$t_a$ (days)	C	O	N	Si	Zn	
As received		93	5	0	2	-*	0.054
	5	90	7	0	2	1	0.078
80	50	88	9	1	1	1	0.102
	100	82	14	3	1	-*	0.171
120	100	80	13	2	4	1	0.163

**Table 3.** Chemical composition of some EPDM samples obtained from XPS wide energy range scan (with permission from [1])

\*traces

The results of curve fitting procedure of the HR C1s are shown in Figure 4. The broad carbon peak in the range of  $E_B$  from 283 eV to 289 eV can be attributed to different carbon-based surface functional groups. C 1s peak was fitted with four Gaussian/ Lorentzian components with the maximum intensity at  $E_B$  of 285 eV, 286.3 eV, 288.1 eV and 289 eV. According to the literature, these energies can be assigned to C-C or C-H, hydroxyl (C-O/ C-OH), carbonyl (C=O) and carboxyl (O-C=O), respectively (see Table 1). Most part of carbon was in form of C-C / C-H. For the samples aged at 80 °C the amount of carbon bonded to oxygen, especially in form of hydroxyl, increased with the increase of ageing duration. After 100 days at 80 °C, carbon-oxygen bonds were composed of hydroxyl (20% with respect to carbon), small portion of carbonyl (4%) and traces of carboxyl (1%). This effect was similar to the evolution of the oxygen content registered in the wide energy range scan (Table 3). Similar behaviour was also observed by [39] and [7]. When comparing the samples aged

during 100 days at 80 °C and 120 °C the portion of carbon-oxygen functional groups was lower at higher temperature, though both samples had similar surface contents of oxygen. According to [39] C-OH bonds are the main product of EPDM ageing as inferred from the C 1s core level peak. However, the results obtained in our work suggested that ageing above 100 °C could cause hydroxyl desorption. This could explain the lower C-O content registered after the treatment at higher temperature.

Variations in the components of the SFE for the elastomer as a function of the ageing parameters were determined using acid-base regression method with the five liquids listed in Table 2. The results are shown in Figure 5. For both ageing temperatures  $\gamma^+$  was statistically insignificant, so this term was omitted from the model. Since the component  $\gamma^+$  is null, EPDM surface is mainly  $\gamma_s^-$  monopolar. In the absence of a parameter of the opposite sign, energy parameters of a monopolar surface do not contribute to the total surface energy (energy of cohesion) since the polar component  $\gamma^{AB} = 2\sqrt{\gamma^+\gamma^-} = 0$  [35]. Therefore, the total SFE is controlled solely by LW interaction. However, monopolar surfaces can strongly interact with bipolar liquids.

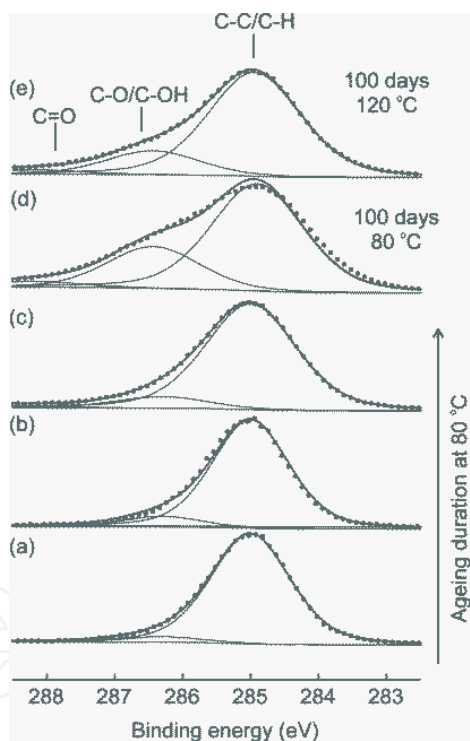


**Figure 4.** C 1s spectra of EPDM: a) as received, b) aged 5 days at 80 °C, c) aged 50 days at 80 °C, d) aged 100 days at 80 °C, e) aged 100 days at 120 °C. Dots – experimental data, solid lines – fitting (with permission from [1])

At 80 °C,  $\gamma_s^{LW}$  increased exponentially with ageing duration reaching almost stable values after 60 days. Parameter  $\gamma_s^-$  had an induction period of approximately 5 days. These results agree with previous works in which the induction period during thermal oxidation of EPDM was determined as 130 h at 80 °C [40] and 150 h at 150 °C [7]. Variations of the induction period in different works can be due to differences in the EPDM composition,

more specifically, in the carbon black and antioxidants content. After induction period,  $\gamma_s^-$  increased rapidly and reached the maximum in 30 days. Then, it remained almost constant with a slightly decreasing tendency, which, however, was within a standard error. The solid line connecting the filled circles in Figure 5a was obtained by fitting the experimental data with an exponential function having a time constant of  $17.7 \pm 0.4$  days.

At 120 °C (Figure 5b),  $\gamma_s^{LW}$  raised up at the beginning of ageing and then followed almost linear increasing behaviour with low rate. Surprisingly, after 100 days ageing at 120 °C  $\gamma_s^{LW}$  was approximately 5% smaller than for ageing at 80 °C. However, after 100 days  $\gamma_s^{LW}$  still maintained the linear growth, while at 80 °C it stabilized.

The evolution of  $\gamma_s^-$  was similar to that of  $\gamma_s^{LW}$ , although the initial increase was not as steep as for  $\gamma_s^{LW}$  component. There is a large difference in the behaviour of  $\gamma_s^-$  for both ageing temperatures. On short ageing periods  $\gamma_s^-$  was notably smaller at the higher temperature, but this difference vanished on large ageing periods. In addition, at 120 °C the induction period was not observed. Probably, the induction period at higher temperature was less than one day, so it could not be measured in these tests. This finding is consistent with [40] who reported shortening of the induction period to 10 h at 120 °C.

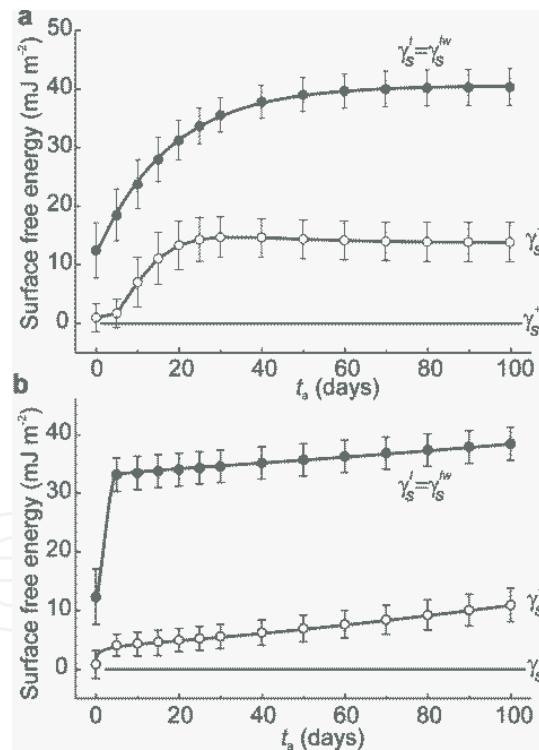


**Figure 5.** Components of SFE as function of ageing duration: a) ageing temperature 80 °C, b) ageing temperature 120 °C (with permission from [1])

The initial value of  $\gamma_s^t$ , which is equal to  $\gamma_s^{LW}$  in our case, is consistent with the findings of [39] for EPDM before weathering test at ambient temperature. They observed that  $\gamma_s^t$  first increased and then stabilized at 23.8 - 25.4 mJ m<sup>-2</sup>. These values are almost two-fold smaller than in our thermal ageing experiments. This fact supports the hypothesis of a

thermally activated nature of the processes responsible for the increase in the surface energy [1].

During ageing of EPDM, two competitive processes typically occur: (i) oxidation of the elastomer chains and (ii) crosslinking between the chains. The oxidation process resides in chain scission and recombination accompanied by formation of oxygen functional groups and radicals. Since double bonds are more chemically active due to the presence of a  $\pi$ -bond, cross-linking and oxidation at the initial stage of ageing mainly involves rupture of double bonds. Characteristic times for cross-linking of EPDM at 80 °C and 120 °C are 100 h and 12.5 h, respectively [40]. After these periods, the material is considered fully cross-linked (at given temperature) that implies significant reduction of the concentration of double bonds. Also, it is reasonable to expect that with the increasing temperature the degree of cross-linking increases and the residual concentration of double bonds decreases. During the induction period, cross-linking is the dominating process as can be inferred from the behaviour of  $\gamma_s^-$ , O/C ratio and very high activation energy for oxidation of EPDM, which ranges between 143.4 and 171.4 kJ mol<sup>-1</sup> [41]. Further ageing of cross-linked elastomer is accompanied with slower oxidation of carbon chains. The higher reactivity of residual double bonds for EPDM aged at 80 °C can explain the steeper increase in SFE and higher concentration of oxygen after induction period. The evolution of SFE for ageing at 80° C is described by a first-order reaction with the activation energy between 63.5 and 83.7 kJ mol<sup>-1</sup>[1]. These values are higher than those reported in [42], but similar to the activation energy for oxidation of long hydrocarbon chain alkanes and aromatics such as in heavy fuel oil [43]. For ageing at 120 °C the linear increase in SFE is described by a zero-order reaction. Zero-order reaction was reported also for surface degradation of fully cross-linked EPDM under artificial weathering conditions [39].

In conclusion, oxygen functional groups, mainly hydroxyl, were identified on EPDM surface after ageing. The presence of these groups was more pronounced after the treatment at 80 °C than at 120 °C. Higher ageing temperatures lead to faster cross-linking processes. At lower temperature C=C bonds are not fully consumed due to cross-linking [3], hence the oxidation processes at lower temperature is more intensive than at higher temperature. In addition, ageing at long durations promotes changes in the surface chemical composition of EPDM. These changes can be attributed to migration of additives towards the surface as reflected by the increase in Si and N concentrations after 100 days ageing at both temperatures.

### **3.2. Characterization of surface chemical composition of elastomer surfaces subject to sliding friction**

Degradation of elastomer surfaces can be accompanied by formation of specific surface texture like smearing or microfibrill formation [44-46]. In [45, 46] it was speculated that these effects could be due to tribochemical reactions and thermooxidative degradation, however no cogent experimental evidences have been presented so far. In order to provide deeper insight into the mechanisms of elastomer failure, surface chemical composition and SFE

were studied before and after friction as a function of the amount of carbon black (CB) filler in EPDM [14]. Carbon black is one of the most widely used reinforcing fillers [47-49] that improves the stiffness and the toughness of rubbers, while maintaining high flexibility and good physical and mechanical properties at low manufacturing costs. The amount of CB varied between 0 and 60 parts per hundred rubber (phr). The samples were subjected to roller-on-plate (ROP) friction tests under conditions detailed in [46]. Friction coefficient was not influenced significantly by the CB content, whereas wear rate decreased with increasing the CB content [14].

Surface chemical composition (at. %) outside and inside the contact zones was determined from the analysis of wide energy XPS spectra (Figure 6). The dominating carbon contribution (95 % and higher) was due to the elastomer backbone structure. The atomic concentrations of other elements including O, Si, S, N and Zn remained below 5 %.

In case some thermooxidative processes and/or tribochemical reactions occur at the contact zone, one can expect certain increase not only in the oxygen concentration, but also in oxygen bonding to carbon atoms in the friction zone. However, the observed behaviour of surface chemical composition was more complex. More specifically, two different tendencies were observed as far as the amount of oxygen in the friction zone is concerned. For unfilled EPDM, the amount of oxygen on the surface of friction zone increased, whereas for filled EPDM it decreased. Notwithstanding these variations, on the surfaces not subjected to friction and for all CB contents, no changes in the binding energy of the oxygen and carbon were observed in high-resolution O 1s and C 1s spectra (Figure 7). The single contribution of C at 285 eV (Figure 7b) from the C-C / C-H component implies absence of oxygen-containing functional groups (see Table 1).

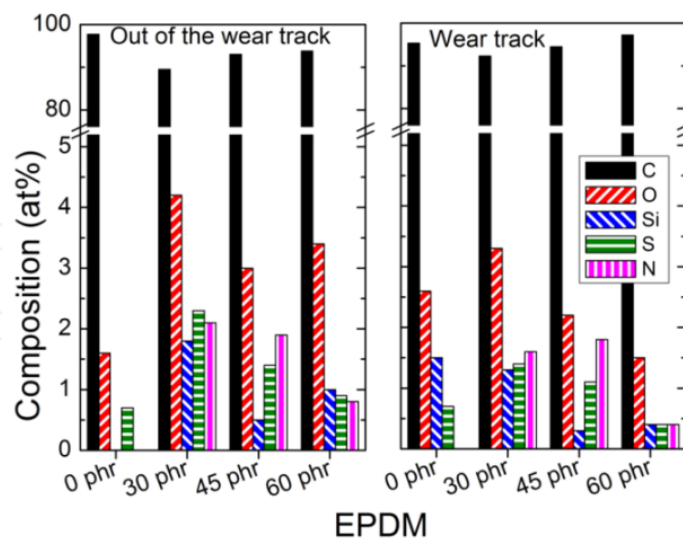


**Figure 6.** Surface composition of EPDM samples with different carbon black content determined from XPS analysis (with permission from [14])

Detailed analysis of the C 1s core level on the surface subjected to friction revealed that FWHM of the peaks were broader for EPDM 0 phr and 30 phr than for EPDM with higher

CB content (Figure 7b). The reason for this broadening could be initially attributed to higher surface roughness of these samples. However, an equivalent broadening did not occur for the O 1s peak. So, roughness could not explain the broadening of the C 1s core level peak. Moreover, the broadening was not completely symmetric and presented a shoulder at lower binding energies. The fitting of the spectra with a single component of the same FWHM for all samples evidenced this asymmetry (Fig. 7d). The shoulder corresponded to energies close to  $sp^2$  carbon [26, 28, 29]. This finding suggests formation of carbon double bonds and/or graphitization in the elastomers with lower CB content. Since these elastomers have worse wear performance, peak broadening can be associated with higher wear rate and damage in the elastomer. A small mismatch between the fitting and the experimental data was observed at higher binding energies only for 0 phr EPDM. This mismatch could be attributed to the roughness effect since the contact surfaces of these samples were severely damaged. In the hypothetical case assuming that this mismatch was caused by C-O bonds, the amount of these species would be rather small. What is clear from these fittings is the absence of carbon-oxygen bonds in the wear track that could explain the different performance in response to friction of the EPDM samples.

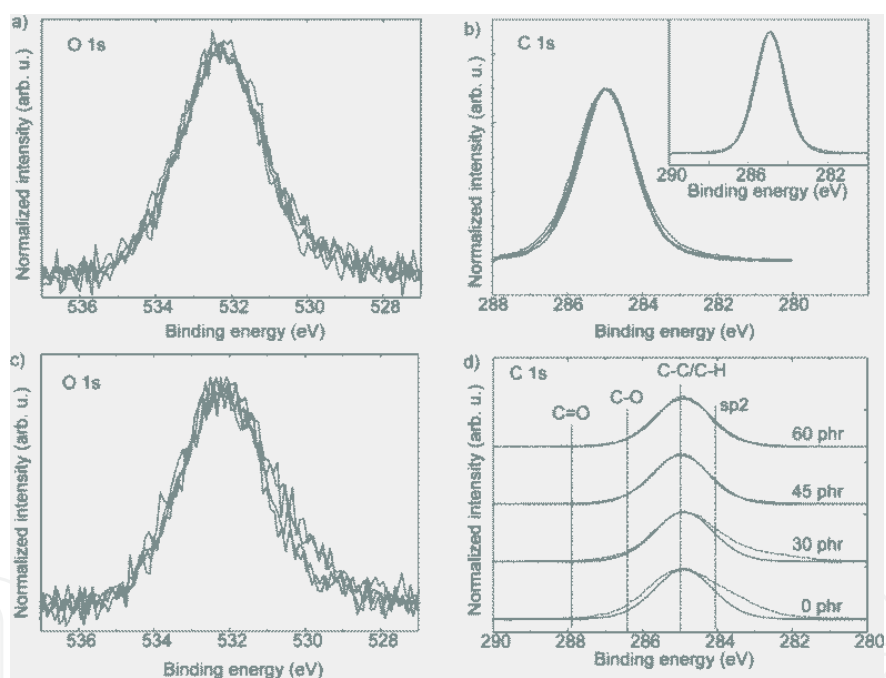


**Figure 7.** HR O 1s and C 1s core level spectra out of (a) and b) and in (c) and d) the wear track of the EPDM samples. Inset in b) represents the fitting of the EPDM 0 phr sample (with permission from [14])

Elastomer degradation is usually associated with bond scission and oxidation of the backbone structure [27, 39]. We argue that oxygen detected on the samples was not related with backbone structure oxidation since no C-O and C=O bonds were observed in XPS spectra. Migration of additives to the surface can be a plausible reason for the increase in oxygen. Actually, silicon was found at the characteristic binding energy of its oxide form (102 eV). Other authors have suggested that fracture of macromolecular chains is accompanied by generation of low molecular weight products as well as C=C structures [27, 50]. For the

samples with larger amounts of CB (45 and 60 phr), the bond scission was smaller as can be inferred from their better wear performance, so the formation of C=C could not be appreciated with the given resolution of the XPS using a non-monochromatic light source.

On the wear track the amount of elements coming from additives (those different from carbon) as well as the amount of oxygen progressively decreased with the increasing amount of carbon black filler. Similarly to the unworn region, oxygen on the worn surface was associated mainly with silicon. Some changes in the sulphur spectrum also occurred. The as-received samples presented two peaks at about 162 eV and 168.5 eV. The first one is related to the S<sup>2-</sup> sulphur state, while the second one is related to higher oxidation states. The peak at 168.5 eV significantly decreased after the removal of airborne contamination indicating superficial localisation of these oxides and the predominant S<sup>2-</sup> state in the wear track. These findings suggested that the sulphur chemical state at the surface of the EPDM samples was altered in the ROP tests, and a part of the oxides located in the outer surface of the elastomer was removed.

Water CAs on worn,  $\theta_{fr,a}$ , and unworn,  $\theta_{nfr}$ , surfaces were measured to study the changes in wettability caused by the presence of new superficial functional groups (mainly oxygen functional groups due to degradation). Subscript *a* denotes the apparent CA. The values of the roughness factor, *r*, and intrinsic CA for water,  $\theta_{fr}$ , are shown in Table 4. For unworn samples, mean value of the CA was around 84° with no significant variations with different carbon black content. However, intrinsic CA was larger on the friction zone than on the unworn surfaces for all samples. The increase in the CA was statistically significant at the significance level 0.05. These findings imply that the worn surfaces were more hydrophobic than the initial ones. This behaviour is opposite to the tendency observed during ageing of a commercial EPDM with 52.6 phr of carbon black, when surface became more hydrophilic with 50% decrease in water CA [1]. The decrease in water CA in [1] was caused by thermooxidation of initially hydrophobic methyl-terminated surface of EPDM. This process was accompanied by an arrangement of polar oxygen functional groups (-C-OH, -C=O) on the outer surface layer [1, 2]. In case of frictional surfaces, no oxidation of the elastomer backbone could be found from XPS spectra. Furthermore, the increase in water CA could be associated with changes in the amount of additives present on the surface. Detailed analysis of the surface chemical composition, scanning electron microscopy and energy-dispersive X-ray spectroscopy revealed increase in zinc oxide and silica at the surface [14]. Both of these oxides have hydrophobic and superhydrophobic properties [51] that can explain the increase in water CA in the friction zone.

CB content (phr)	<i>r</i>	$\theta_{fr}$ (deg)	$se\theta_{fr}$ (deg)	$\theta_{nfr}$ (deg)	$se\theta_{nfr}$ (deg)
0	1.654	107	4.98	81	3.9
30	1.102	90.6	2.11	84	2.1
45	1.207	99.3	2.46	85	1.1
60	1.129	104	4.39	84	2.9

**Table 4.** Roughness factor (*r*), mean intrinsic contact angles on worn,  $\theta_{fr}$ , and unworn,  $\theta_{nfr}$ , surfaces with corresponding standard errors of mean (with permission from [14])

From the results of XPS and CA measurements we concluded that no thermooxidation processes were observed on friction zone under given experimental conditions for all EPDM samples and irrespective of the CB content. Chemical modification of the EPDM surface was due to mechanochemical effects rather than a thermooxidative effect [52-55]. Softer EPDMs with lower carbon black content were severely damaged during ROP test. The increase in C=C bonds for these samples can be attributed to bonds breaking accompanied by different radical reactions [56-58].

### **3.3. Characterization of surface chemical composition after atmospheric plasma treatments and thin coating of amorphous diamond-like carbon (DLC)**

Surface modification is aimed at changing the characteristics of the surface and thin subsurface layer [59] or generation of active centres for further attachment of compounds [60]. By surface modification desired surface properties such as adhesion or wettability [61] can be obtained leaving the underlying bulk unchanged. By doing so, both the surface and bulk properties can be independently tailored and optimized. In this section we present some case studies with the purpose of demonstration the capabilities of XPS technique.

Plasma processing of materials is a crucial industrial technology in many areas including electronics, aerospace, automotive, and biomedical industries [62] due to its versatility [63]. Though nowadays plasma processing is performed mostly at low pressures, atmospheric plasma systems provide an appealing alternative to vacuum plasma systems because continuous processing can be performed at a lower cost [62, 64-66]. Operation under atmospheric pressure provides high flexibility and portability to this technique [32] and allows it expansion to processing of a larger number of materials [62]. One of the possibilities of atmospheric plasma treatments is the use of a plasma torch [67]. In this case, a reactive gas is added to the primary feed gas of the plasma torch in order to generate a flux of chemically active species, e.g. fluorine, toward treated surface. In this way, the surface being fluorinated should not be immersed in reagents and is not directly exposed to the plasma [62]. This treatment can be performed at room temperature and is faster than other fluorination methods [68]. All these advantages are important for industrial application. In our studies surface modification was carried out in two ways: using only ions of inert gases or using also chemically active gases. The reactive gases used for fluorination (commonly SF<sub>6</sub> and CF<sub>4</sub>) should be thoroughly diluted with a carrier gas in order to create a stable plasma at atmospheric pressure. Nitrogen, argon or helium are typically used as a carrier gas as they can be easily ionized [65]. Due to the high reactivity of ionized fluorine-containing gases, surface reactions, etching, and plasma polymerization can occur simultaneously. The predominance of one or another will depend on the gas feed, the operating parameters and the chemical nature of the polymer substrates.

Table 5 shows the chemical composition of EPDM elastomers modified by atmospheric plasma using N<sub>2</sub>, Ar and He carrier gases in combination with SF<sub>6</sub> and CF<sub>4</sub> fluorination precursors. The composition of untreated elastomers and those activated only by He plasma are included for comparison. The chemical composition was determined from XPS analysis.

All plasma-treated samples had fluorine (0.3 to 13 at. %), oxygen (13 to 22 at. %) and nitrogen (< 2 at. %) on their surfaces. It should be mentioned that plasma treatments promoted a significant increase in the oxygen content. This oxygen incorporation into the surface was similar when plasma activation only with He gas was used. Therefore, oxygen content on the treated surfaces does not significantly depend on the presence or absence of reactive gases during plasma treatments. Oxygen incorporation to the elastomer takes place through interactions between free radicals, O<sub>2</sub> and H<sub>2</sub>O molecules from ambient air after the plasma treatment [64]. Traces of sulphur were detected on the EPDM surface after plasma processing using SF<sub>6</sub> [69]. The degree of fluorination for each treatment can be evaluated from O/C and F/C atomic ratios shown in Table 5. From these data it is evident that for fluorination purposes CF<sub>4</sub> is more effective than SF<sub>6</sub>. Previously, these results were explained in terms of the dissociation products formed in the plasma [32, 66]. No significant differences in F/C ratio were found for the combination of inert carrier gases (Ar and He) and CF<sub>4</sub>, whereas He was more effective for fluorination in combination with SF<sub>6</sub>. At the same time, nitrogen carrier gas yielded lower F/C ratio. This is because radicals produced by dissociation of SF<sub>6</sub> and CF<sub>4</sub> could not react with N<sub>2</sub> due to the strong bond between nitrogen atoms. So far, only few information is available in the literature on these reactions [70, 71] to allow definite conclusion. The analysis of the HR C 1s (Figure 2 a, b) revealed the changes in the shape of the core level peak that evidenced not only significant increase in the C-O bonds after the fluorination treatments, but also the apparition of new functional groups involving carbon, oxygen and fluorine.

Process	Chemical composition (at. %)							
	C	O	N	F	S	F/C	O/C	
Untreated	93	5	0	0	0	0	0.005	
SF <sub>6</sub>	N <sub>2</sub>	80.4	16.3	1.5	1.3	0.5	0.02	0.20
	Ar	81.6	14.1	1.9	1.7	0.6	0.02	0.17
	He	71.1	19.6	1.6	6.8	0.9	0.09	0.27
CF <sub>4</sub>	N <sub>2</sub>	84.4	13.4	1.9	0.3	0	0.003	0.16
	Ar	65.9	19.3	1.8	13.0	0	0.20	0.29
	He	63.4	21.9	1.8	12.0	0	0.19	0.34
Activation	He	79	16	traces	-	-	-	0.20

**Table 5.** Surface composition of EPDM samples after atmospheric plasma treatments

	C1s core level components						
	C-C C-H	C-O -C-H-CF <sub>2</sub>	C=O CH-CF	O-C=O CFH-CF <sub>2</sub>	CF	CF <sub>2</sub>	CF <sub>3</sub>
Untreated	96	4	0	0	0	0	0
He activation	77	12	8	3	0	0	0
Fluorinated	45	36	7	5	3	3	1

**Table 6.** Analysis of the components of the C1s core level of EPDM elastomers: untreated, He activated and fluorinated

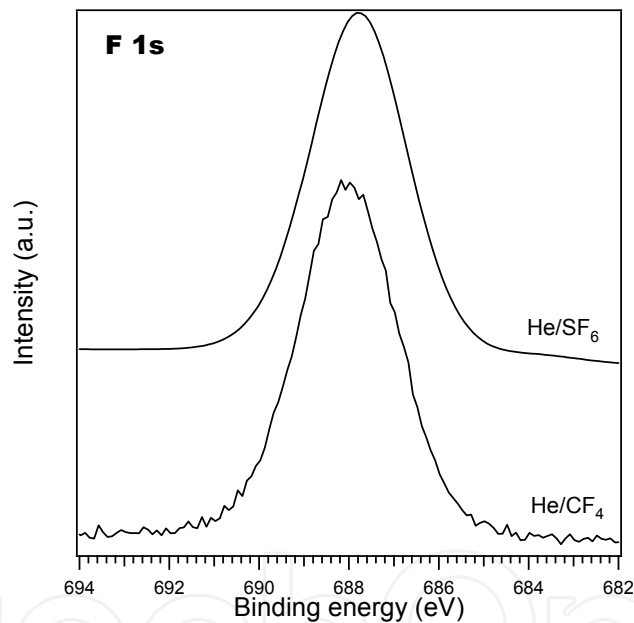
The presence of CF and CF<sub>2</sub> can be explained by H substitution and chain scissions [32]. CF<sub>2</sub>- represents the main chain of the polymer, -CF- component could indicate cross-link sites [72] and -CF<sub>3</sub> component indicates end groups of polymer chains [72] and grafting [32]. These findings imply enhancing of cross-linking in the elastomer due to plasma processing with fluorine-containing gas.

Figure 2b and 2c show a comparison of HR C1s for elastomers treated with CF<sub>4</sub> and SF<sub>6</sub> using the same carrier gas. From the shape of the peaks one can observe again that CF<sub>4</sub> is more effective than SF<sub>6</sub> in fluorinating because of the presence of additional fluorine containing groups together with the increase in the total fluorine content already mentioned in Table 6. SF<sub>6</sub> molecules mainly dissociate into fluorine atoms and SF<sub>5</sub> radicals [66], whereas CF<sub>4</sub> produces fluorine, CF, CF<sub>2</sub> and CF<sub>3</sub> radicals that react with the elastomer surface leading to a substantial incorporation of fluorine [32]. Though fluorine atoms were considered as the main responsible of the fluorination process, CF<sub>x</sub> radicals could contribute to formation of highly fluorinated components (in particular CF<sub>3</sub> groups) [65]. Thus, higher content of CF<sub>x</sub> groups after treatment with CF<sub>4</sub> in comparison to SF<sub>6</sub> could be attributed to the larger number of fluorine-containing radicals. Our results demonstrated that the main effect of SF<sub>6</sub> resided in oxidation of the polymer surface, while CF<sub>4</sub>, in addition to surface oxidation also induced incorporation of CF<sub>x</sub> radicals enhancing the efficiency of the fluorination process [4]. SFE measurements of fluorinated samples revealed that increase in the surface free energy,  $\gamma$ , was noticeable only for the samples which chemical composition was significantly modified, especially by incorporation of oxygen and fluorine polar groups. The increase in SFE related mainly with the electron donor,  $\gamma$ , contribution of the polar component,  $\gamma^{AB}$ , [73].

It should be noted that the modification of elastomer surface is not always as evident as in the above examples. The extent of surface modification induced by a particular surface treatment is highly dependent on the type of the elastomer. For instance, when the same treatment is carried out for HNBR, the extent of the surface modification was much less as compared with EPDM (Figure 2d). Surface chemical composition of treated HNBR was almost the same as for untreated one with no presence of fluorine containing groups and no increase in oxygen content [15]. A saturated backbone structure of elastomer such as HNBR makes it less reactive to the plasma treatments.

From systematic studies of fluorinating process under different conditions we concluded that high concentration of fluorine on the elastomer surface, typically higher than 7%, is associated with formation of fluorine-containing functional groups in form of CF, CF<sub>2</sub> or CF<sub>3</sub>. The presence of CF and CF<sub>2</sub> can be explained by H substitution and chain scissions [32], where -CF<sub>2</sub>- represents the main chain of the polymer, -CF- component could indicate cross-link sites [72], and -CF<sub>3</sub> component indicates end groups of polymer chains [72] and grafting [32]. These findings imply enhancing of cross-linking in the elastomer due to plasma processing with fluorine-containing gas. On the contrary, in processing with lower fluorinating efficiency (< 7%) no evidence of C-F bonds was found [4].

The analysis of other core levels such as O 1s or F 1s can provide complementary information on surface chemical groups. From the analysis of O 1s core level peak of fluorinated samples having one symmetric peak at about 532.6 eV (not shown here, see [4]), we concluded that hydroxyl or ether species were predominant after all fluorinating treatments [62]. This finding is in agreement with the C 1s analysis presented above, as can be inferred from small contributions in the C 1s peak from carboxyl and carbonyl species at 288.1 and 289 eV, respectively [26]. On the other hand, F 1s core level spectra had certain differences when using SF<sub>6</sub> and CF<sub>4</sub> with the same carrier gas, e.g. He (Figure 8). When SF<sub>6</sub> was used, the peak was symmetric and centred at about 687.2 eV, whereas for CF<sub>4</sub> it was centred at 688.1 eV. These energies are close to those reported in the literature for fluorine covalently bonded to carbon [62, 64]. These findings clearly indicated an incorporation of fluorine in the polymer chains. The behaviour observed in the F 1s peaks presented a good correlation with the C 1s analysis given above. Higher fluorine concentration in the sample is associated with the presence of CF<sub>2</sub> bonds according to the C 1s analysis and displacement of the main F 1s peak towards higher binding energies [26].



**Figure 8.** Comparison of the F 1s core level after fluorination treatments with different precursors

Another way to modify elastomer surfaces and improve their tribological properties consists in application of different coatings. Elastomer surfaces with low friction can be obtained by deposition of (3-aminopropyl)-triethoxysilane (APEO) or (3-glycidoxypropyl)trimethoxysilane (GLYMO) coatings using siloxane precursors [74, 75] or polytetrafluoroethylene (PTFE). PTFE is commonly used as a coating on metallic substrates and it has been recently optimised for use on elastomers yielding low friction coefficient and enhancing other properties [75, 76]. Diamond like carbon (DLC) is another very promising candidate for coatings due to its excellent tribological properties and chemical inertness [6]. DLC coatings have been widely used on different substrates including metals, ceramics and other inorganic materials. Recently, elastic DLC coating on elastomers was developed [5]. Initially,

the idea of applying a hard DLC film on soft elastomer materials with low elastic modulus received much scepticism because of the risk of loss of adherence and interfacial delamination. However, after successful demonstration of the efficiency of DLC coatings on elastomer substrates their application has been widely spread, especially in automotive industry. Further advances in application of DLC on elastomer surfaces can be made on the basis of deeper understanding of surface chemistry of coated systems. In this work we studied surface chemical composition of uncoated and DLC-coated NBR and HNBR elastomers using XPS and CA methods. HNBR is a hydrogenated elastomer with no double bonds in the elastomer backbone structure. Therefore, HNBR is less chemically reactive than NBR against the same treatment [4].

Surface chemical composition of elastomers obtained from the wide energy range scan XPS spectra are shown on Table 7. For all samples, carbon, oxygen and nitrogen were the main surface elements. Small amounts of other elements used in the elaboration processes of elastomers were also detected [22]. As we already mentioned before, these components have no important influence on the surface properties [13]. When DLC coating was applied, oxygen content slightly increased. In order to investigate changes in the main bonding of the elastomers, curve fitting procedure of XPS spectra of the C1s core level peaks was performed (see Figure 9 and Table 7). Four components: C-C/CH; C-O; C=O and O-C=O were used for fitting. These components were derived from the expected chemistry of the samples and taking into account natural oxidation process of the elastomers. The binding energies of these components are listed in Table 1. CN bond from the NBR structure was not considered due to the small contribution of nitrogen to the final composition. The results evidenced that C-C contribution corresponding to the backbone structure of the elastomers decreased for DLC-coated elastomers as a consequence of the formation of oxygen functional groups, mainly in form of C-O. HNBR presented larger variation of the carbon bond than NBR.

Despite the small variations observed in the surface chemical composition, DLC-coated elastomers presented better tribological performance reflected in a significant reduction in the coefficient of friction (COF) and friction noise [77]. Also, water CA increased for NBR after DLC deposition (Figure 10) indicating the increase in the hydrophobic character of NBR elastomer surfaces after DLC deposition. This finding is consistent with previous works where an increase in the hydrophobic properties of the DLC-coated elastomers was attributed to  $sp^2$  and  $sp^3$  hybridised carbon bonds in the DLC coating. One should bear in mind that higher hydrophobicity of the surface is usually related to a higher chemical stability. Actually, in our experiments SFE of NBR elastomers decreased by 9% after DLC deposition [77]. For hydrogenated HNBR elastomer, the variations in the hydrophobicity after DLC coatings were statistically insignificant. In contrast to NBR, SFE increased by 8% for DLC-coated HNBR. We suggested that hydrogenation of unsaturated bonds to form HNBR results in different reactivity of the elastomer towards the DLC coatings. Despite the fact that the same type of DLC coating was deposited on all the elastomers, the extent of the modifications was different depending on the substrate.

	C1s core level components						
	C	O	N	C-C C-H	C-O	C=O	O-C=O
NBR uncoated	98	1	0	97	3	0	0
NBR coated	98	1	0	93	7	0	0
HNBR uncoated	92	4	3	91	5	4	0
HNBR coated	89	6	3	86	11	2	1

**Table 7.** Surface composition and analysis of the components of the C1s core level of NBR and HNBR before and after DLC coating

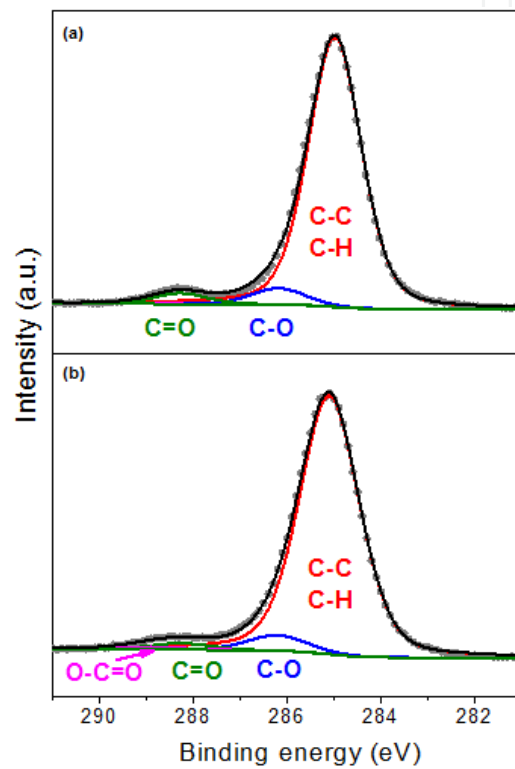


**Figure 9.** HRC 1s core level of HNBR elastomer before (a) and after DLC coating (b)

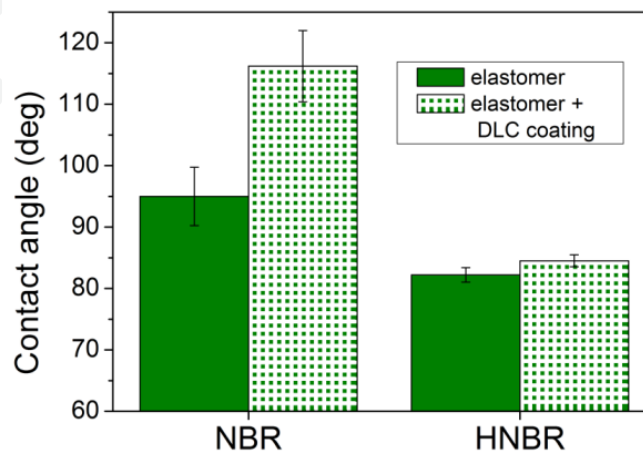


**Figure 10.** Water CA on elastomers before and after DLC coating

## 4. Concluding remarks

We have shown that XPS is a sensitive and versatile technique to characterize surface chemical composition of engineered elastomer surfaces. The combination of XPS with other techniques such as CA measurements or SFE calculations allows the evaluation of minute changes in surface chemical composition and structure of surface functional groups resulting from surface degradation or surface treatment. Therefore, factors like ageing processes, lubricant absorption or reaction of the elastomer chains under surface treatment have been analysed with this technique. As XPS binding energies are not only element-specific but also contain chemical information, it provides information about chemical states of a particular element. So, the degradation of the elastomer backbone structure during ageing and wear was evaluated in terms of C-O or C-OH bond formation. In general, the binding energy increases with increasing oxidation state and, for a fixed oxidation state, with the electronegativity of the ligands. The C 1s spectrum of fluorocarbon polymer is an example how the binding energy of carbon depends sensitively on the electronegativity of its neighbours. It was shown that an increase in the oxygen content is not necessarily related to oxidation of carbon bonds and, therefore, to degradation. The presence of new elements, e.g. fluorine due to plasma fluorination, is not always related to the formation of C-F bonds as well. This information cannot be obtained by many other analytical techniques, which makes XPS particularly interesting for this kind of studies. One limitation found was the lack of sensitivity to resolve the possible cross-linking after certain surface treatments. The energy gap between the C=C and C-C bonds are below 0.8 eV which is the range of resolution of nonmonochromated Mg K $\alpha$  X-ray source. However, cross-linking effects were determined from the variation of SFE components and O/C and F/C ratios. When studying elastomer surfaces subjected to rubbing, no important oxidation indicative of thermochemical reactions was observed. Modifications of the elastomer surfaces were interpreted in terms of mechanochemical reactions and wear.

The final properties of elastomer components can be significantly modified even by small changes in chemical composition of thin surface layer. The extent of the surface modification is clearly influenced by the elastomer substrate and it is more significant for organic materials than other inorganic materials.

## Author details

Lidia Martínez and Elisa Román

*ICMM-CSIC, Dept. Surfaces and Coatings, Madrid, Spain*

Roman Nevshupa\*

*CISDEM-CSIC, Spain*

---

\* Corresponding Author

## Acknowledgement

Most of this study was developed under the framework of the EU project KRISTAL No. 515837-2 (6<sup>th</sup> FP). The authors acknowledge Dr. Yves Huttel for his fruitful discussion about the XPS results, IVW (Germany) and TRW (Spain) for the EPDM substrates, VITO (Belgium) for the plasma treatments, HEF (France) for the DLC coatings. The authors also acknowledge the Spanish National Research Council (CSIC) for grant PIE201160E085 and Spanish Ministry for Economy and Competitiveness for financial support provided in the projects MAT2011-29194-C02-02, BIA2011-25653 and "Ramón y Cajal" RYC-2009-04125.

## 5. References

- [1] Nevshupa R, Martinez L, Alvarez L, Lopez MF, Huttel Y, Mendez J, et al. (2011) Influence of thermal ageing on surface degradation of ethylene-propylene-diene elastomer. *Journal of Applied Polymer Science*. 119:242-251.
- [2] Laoharajanaphand P, Lin TJ, Stoffer JO (1990) Glow discharge polymerization of reactive functional silanes on poly(methyl methacrylate). *Journal of Applied Polymer Science*. 40:369-384.
- [3] Desai SM, Bodas DS, Singh RP (2004) Fabrication of long-term hydrophilic elastomeric surfaces via plasma induced surface cross-linking of functional monomers. *Surface and Coatings Technology*. 184:6-12.
- [4] Martínez L, Huttel Y, Verheyde B, Vanhulsel A, Román E (2010) Photoemission study of fluorination atmospheric pressure plasma processes on EPDM: Influence of the carrier and fluorinating gas. *Applied Surface Science*. 257:832-836.
- [5] Nakahigashi T, Tanaka Y, Miyake K, Oohara H (2004) Properties of flexible DLC film deposited by amplitude-modulated rf p-cvd. *Tribology International*. 37:907-912.
- [6] Lindholm P, Björklund S, Svahn F (2006) Method and surface roughness aspects for the design of DLC coatings. *Wear*. 261:107-111.
- [7] Delor-Jestin F, Lacoste J, Barrois-Oudin N, Cardinet C, Lemaire J (2000) Photo-, thermal and natural ageing of ethylene-propylene-diene monomer (EPDM) rubber used in automotive applications. Influence of carbon black, crosslinking and stabilizing agents. *Polymer Degradation and Stability*. 67:469-477.
- [8] Majumder PS, Bhowmick AK (1998) Friction behaviour of electron beam modified ethylene-propylene diene monomer rubber surface. *Wear*. 221:15-23.
- [9] Lonkar SP, Kumar AP, Singh RP (2007) Photo-stabilization of EPDM-clay nanocomposites: Effect of antioxidant on the preparation and durability. *Polymers for Advanced Technologies*. 18:891-900.
- [10] Farahani TD, Bakhshandeh GR (2005) The effect of curing on sorption and diffusion of a brake fluid in EPDM elastomer. *e-Polymers*. 47:1-10.
- [11] Banik I, Bhowmick AK (2000) Electron beam modification of filled fluorocarbon rubber. *Journal of Applied Polymer Science*. 76:2016-2025.

- [12] Tillier DL, Meuldijk J, Koning CE (2003) Production of colloiddally stable latices from low molecular weight ethylene–propylene–diene copolymers. *Polymer*. 44:7883-7890.
- [13] Degrange JM, Thomine M, Kapsa P, Pelletier JM, Chazeau L, Vigier G, et al. (2005) Influence of viscoelasticity on the tribological behaviour of carbon black filled nitrile rubber (NBR) for lip seal application. *Wear*. 259:684-692.
- [14] Martinez L, Nevshupa R, Felhoes D, de Segovia JL, Roman E (2011) Influence of friction on the surface characteristics of EPDM elastomers with different carbon black contents. *Tribology International*. 44:996-1003.
- [15] Martínez L, Álvarez L, Huttel Y, Méndez J, Román E, Vanhulsel A, et al. (2007) Surface analysis of NBR and HNBR elastomers modified with different plasma treatments. *Vacuum*. 81:1489-1492.
- [16] Alisoy HZ, Baysar A, Alisoy GT (2005) Physicomathematical analysis of surface modification of polymers by glow discharge in medium. *Physica A: Statistical Mechanics and its Applications*. 351:347-357.
- [17] Einstein A (1905) Über einen die erzeugung und verwandlung des lichtes betreffenden heuristischen gesichtspunkt. *Annalen der Physik*. 322:132-148.
- [18] Hüfner S (2003) Photoelectron spectroscopy. Principles and applications, 3rd edition. Berlin: Springer, 662 p.
- [19] Seah MP, Dench WA (1979) Quantitative electron spectroscopy of surfaces: A standard data base for electron inelastic mean free paths in solids. *Surface and Interface Analysis*. 1:2-11.
- [20] Briggs D, Seah MP (1990) Practical surface analysis—auger and X-ray photoelectron spectroscopy. Chichester: Wiley, 657 p.
- [21] Woodruff DP, Delchar TA (1986) Modern techniques of surface science. Cambridge: Cambridge University Press, 608 p.
- [22] Mitra S, Ghanbari-Siahkali A, Kingshott P, Rehmeier HK, Abildgaard H, Almdal K (2006) Chemical degradation of crosslinked ethylene-propylene-diene rubber in an acidic environment. Part i. Effect on accelerated sulphur crosslinks. *Polymer Degradation and Stability*. 91:69-80.
- [23] Akhter S, Allan K, Buchanan D, Cook JA, Champion A, White JM (1988) XPS and IR study of X-ray induced degradation of pva polymer film. *Applied Surface Science*. 35:241-258.
- [24] Coullerez G, Chevolut Y, Léonard D, Xanthopoulos N, Mathieu HJ (1999) Degradation of polymers (PVC, PTFE, m-f) during X-ray photoelectron spectroscopy (ESCA) analysis. *Journal of Surface Analysis*. 5:235-239.
- [25] Shirley DA (1972) High-resolution x-ray photoemission spectrum of the valence bands of gold. *Physical Review B*. 5:4709-4714.
- [26] Beamson G, Briggs D (1992) High resolution XPS for organic polymers: The Scienta ESCA 300 database. Ney York: John Wiley & Sons, 306 p.
- [27] Zhang SW (2004) Tribology of elastomers. Amsterdam: Elsevier, 282 p.

- [28] Swaraj S, Oran U, Lippitz A, Friedrich JF, Unger WES (2005) Surface analysis of plasma-deposited polymer films, 6. *Plasma Processes and Polymers*. 2:572-580.
- [29] Grythe KF, Hansen FK (2006) Surface modification of EPDM rubber by plasma treatment. *Langmuir*. 22:6109-6124.
- [30] Nansé G, Papirer E, Fioux P, Moguet F, Tressaud A (1997) Fluorination of carbon blacks: An X-ray photoelectron spectroscopy study: I. A literature review of XPS studies of fluorinated carbons. XPS investigation of some reference compounds. *Carbon*. 35:175-194.
- [31] Wen C-H, Chuang M-J, Hsiue G-H (2006) Plasma fluorination of polymers in glow discharge plasma with a continuous process. *Thin Solid Films*. 503:103-109.
- [32] Hochart F, Levalois-Mitjaville J, De Jaeger R, Gengembre L, Grimblot J (1999) Plasma surface treatment of poly(acrylonitrile) films by fluorocarbon compounds. *Applied Surface Science*. 142:574-578.
- [33] Wenzel RN (1936) Resistance of solid surfaces to wetting by water. *Industrial & Engineering Chemistry*. 28:988-994.
- [34] Gao L, McCarthy TJ (2007) How Wenzel and Cassie were wrong. *Langmuir*. 23:3762-3765.
- [35] Van Oss CJ, Chaudhury MK, Good RJ (1988) Interfacial Lifshitz-van der Waals and polar interactions in macroscopic systems. *Chemical Reviews*. 88:927-941.
- [36] Wu W, Giese RF, Jr., van Oss CJ (1995) Evaluation of the Lifshitz-van der Waals/acid-base approach to determine surface tension components. *Langmuir*. 11:379-382.
- [37] Navrátil Z, Buršíková V, St'ahel P, Šíra M, Zvěřina P (2004) On the analysis of surface free energy of DLC coatings deposited in low pressure rf discharge. *Czechoslovak Journal of Physics*. 54:C877-C882.
- [38] Luner PE, Oh E (2001) Characterization of the surface free energy of cellulose ether films. *Colloids and Surfaces A: Physicochemical and Engineering Aspects*. 181:31-48.
- [39] Zhao Q, Li X, Gao J (2008) Surface degradation of ethylene-propylene-diene monomer (EPDM) containing 5-ethylidene-2-norbornene (ENB) as diene in artificial weathering environment. *Polymer Degradation and Stability*. 93:692-699.
- [40] Kumar A, Commereuc S, Verney V (2004) Ageing of elastomers: A molecular approach based on rheological characterization. *Polymer Degradation and Stability*. 85:751-757.
- [41] Mason LR, Reynolds AB (1998) Comparison of oxidation induction time measurements with values derived from oxidation induction temperature measurements for EPDM and XLPE polymers. *Polymer Engineering & Science*. 38:1149-1153.
- [42] Budrugaec P, Segal E (1994) On the kinetics of the thermal degradation of polymers with compensation effect and the dependence of activation energy on the degree of conversion. *Polymer Degradation and Stability*. 46:203-210.
- [43] Ayala JA, Rincón ME (1981) The oxidation of fuel oil #6 studied by differential scanning calorimetry. *ACS Fuel*. 26:120-130.
- [44] Schallmach A (1971) How does rubber slide? *Wear*. 17:301-312.

- [45] Felhös D, Karger-Kocsis J (2008) Tribological testing of peroxide-cured EPDM rubbers with different carbon black contents under dry sliding conditions against steel. *Tribology International*. 41:404-415.
- [46] Karger-Kocsis J, Mousa A, Major Z, Békési N (2008) Dry friction and sliding wear of EPDM rubbers against steel as a function of carbon black content. *Wear*. 264:359-367.
- [47] Rathinasamy P, Balamurugan P, Balu S, Subrahmanian V (2004) Effect of adhesive-coated glass fiber in natural rubber (NR), acrylonitrile rubber (NBR), and ethylene-propylene-diene rubber (EPDM) formulations. I. Effect of adhesive-coated glass fiber on the curing and tensile properties of NR, NBR, and EPDM formulations. *Journal of Applied Polymer Science*. 91:1111-1123.
- [48] Chou H-W, Huang J-S, Lin S-T (2007) Effects of thermal aging on fatigue of carbon black-reinforced EPDM rubber. *Journal of Applied Polymer Science*. 103:1244-1251.
- [49] Wang M-J, Wolff S. Surface energy of carbon black. In: Donnet J-B, editor. *Carbon black: Science and technology*, second edition. Ney York: CRC Press; 1993. p. 289-355.
- [50] Rizk RAM, Abdul-Kader AM, Ali ZI, Ali M (2009) Effect of ion bombardment on the optical properties of Idpe/EPDM polymer blends. *Vacuum*. 83:805-808.
- [51] Zhang J, Huang W, Han Y (2006) Wettability of zinc oxide surfaces with controllable structures. *Langmuir*. 22:2946-2950.
- [52] Nevshupa R, Roman E, de Segovia JL (2010) Model of the effect of local frictional heating on the tribodesorbed gases from metals in ultra-high vacuum. *International Journal of Materials & Product Technology*. 38:57-65.
- [53] Nevshupa RA (2009) The role of athermal mechanisms in the activation of tribodesorption and triboluminescence in miniature and lightly loaded friction units. *Journal of Friction and Wear*. 30:118-126.
- [54] Heinike G (1984) *Tribochemistry*. Munchen: Carl Hanser Verlag, 495 p.
- [55] Kostetsky BI (1992) The structural-energetic concept in the theory of friction and wear (synergism and self-organization). *Wear*. 159:1-15.
- [56] Malhotra M, Kumar S (1997) Thermal gas effusion from diamond-like carbon films. *Diamond and Related Materials*. 6:1830-1835.
- [57] Butyagin PY (1971) Kinetics and nature of mechanochemical reactions. *Russian Chemical Reviews*. 40:901-915.
- [58] Butyagin PY (1984) Structural disorder and mechanochemical reactions in solids. *Russian Chemical Reviews*. 53:1025-1038.
- [59] Orellana LM, Pérez FJ, Gómez C (2005) The effect of nitrogen ion implantation on the corrosion behaviour of stainless steels in chloride media. *Surface and Coatings Technology*. 200:1609-1615.
- [60] Goddard JM, Hotchkiss JH (2007) Polymer surface modification for the attachment of bioactive compounds. *Progress in Polymer Science*. 32:698-725.
- [61] Minko S, Müller M, Motornov M, Nitschke M, Grundke K, Stamm M (2003) Two-level structured self-adaptive surfaces with reversibly tunable properties. *Journal of the American Chemical Society*. 125:3896-3900.

- [62] Ho KKC, Lee AF, Bismarck A (2007) Fluorination of carbon fibres in atmospheric plasma. *Carbon*. 45:775-784.
- [63] Mitra S, Ghanbari-Siahkali A, Kingshott P, Rehmeier HK, Abildgaard H, Almdal K (2006) Chemical degradation of crosslinked ethylene-propylene-diene rubber in an acidic environment. Part ii. Effect of peroxide crosslinking in the presence of a coagent. *Polymer Degradation and Stability*. 91:81-93.
- [64] Felten A, Ghijsen J, Pireaux JJ, Johnson RL, Whelan CM, Liang D, et al. (2008) Photoemission study of CF<sub>4</sub> rf-plasma treated multi-wall carbon nanotubes. *Carbon*. 46:1271-1275.
- [65] Fanelli F, Fracassi F, d'Agostino R (2008) Fluorination of polymers by means of he/CF<sub>4</sub>-fed atmospheric pressure glow dielectric barrier discharges. *Plasma Processes and Polymers*. 5:424-432.
- [66] Borisov S, Khotimsky VS, Rebrov AI, Rykov SV, Slovetsky DI, Pashunin YM (1997) Plasma fluorination of organosilicon polymeric films for gas separation applications. *Journal of Membrane Science*. 125:319-329.
- [67] <http://www.vitoplasma.com/en/30>, last access on March 2012.
- [68] Yasuda H, Hsu TS (1977) Some aspects of plasma polymerization of fluorine-containing organic compounds. *Journal of Polymer Science: Polymer Chemistry Edition*. 15:2411-2425.
- [69] Barni R, Riccardi C, Selli E, Massafra MR, Marcandalli B, Orsini F, et al. (2005) Wettability and dyeability modulation of poly(ethylene terephthalate) fibers through cold SF<sub>6</sub> plasma treatment. *Plasma Processes and Polymers*. 2:64-72.
- [70] Kumar SVK, Sathyamurthy N, Manogaran S, Mitra SK (1994) Possible reaction of atomic nitrogen with SF<sub>x</sub> (x = 1-5) and CF<sub>x</sub> (x = 1-3) fragments from N<sub>2</sub>-SF<sub>6</sub> and N<sub>2</sub>-CF<sub>4</sub> discharges. *Chemical Physics Letters*. 222:465-470.
- [71] Radoiu MT (2003) Studies of 2.45 GHz microwave induced plasma abatement of CF<sub>4</sub>. *Environmental Science & Technology*. 37:3985-3988.
- [72] Tran ND, Dutta NK, Roy Choudhury N (2006) Weatherability and wear resistance characteristics of plasma fluoropolymer coatings deposited on an elastomer substrate. *Polymer Degradation and Stability*. 91:1052-1063.
- [73] Schlögl S, Kramer R, Lenko D, Schröttner H, Schaller R, Holzner A, et al. (2011) Fluorination of elastomer materials. *European Polymer Journal*. 47:2321-2330.
- [74] Verheyde B, Havermans D, Vanhulsel A (2011) Characterization and tribological behaviour of siloxane-based plasma coatings on HNBR rubber. *Plasma Processes and Polymers*. 8:755-762.
- [75] Verheyde B, Rombouts M, Vanhulsel A, Havermans D, Meneve J, Wangenheim M (2009) Influence of surface treatment of elastomers on their frictional behaviour in sliding contact. *Wear*. 266:468-475.
- [76] <http://www.fluoroprecision.co.uk/ptfe-coated-elastomers-rubbers.html>, last access on March 2012.

- [77] Martinez L, Nevshupa R, Alvarez L, Huttel Y, Mendez J, Roman E, et al. (2009) Application of diamond-like carbon coatings to elastomers frictional surfaces. *Tribology International*. 42:584-590.

IntechOpen

IntechOpen